Green Chemistry

Sustainable Potassium Sorbate Production from Triacetic Acid Lactone in Food-grade Solvents

Journal:	*Green Chemistry*
Manuscript ID	GC-ART-09-2024-004832.R2
Article Type:	Paper
Date Submitted by the Author:	24-Apr-2025
Complete List of Authors:	Kim, Min Soo; University of Wisconsin-Madison, Chemical and Biological Engineering Bhagwat, Sarang; University of Illinois at Urbana-Champaign, Civil and Environmental Engineering Santiago-Martínez, Leoncio; University of Wisconsin, Department of Chemical and Biological Engineering; University of Illinois at Urbana-Champaign, Shi, Xiaolei; University of Wisconsin-Madison, Chemical and Biological Engineering Choi, Kyuhyeok ; University of Wisconsin-Madison, Chemical and Biological Engineering Guest, Jeremy; University of Illinois at Urbana-Champaign, Civil & Environmental Engineering Huber, George; University of Wisconsin, Chemical and Biological Engineering

Green Foundation

1. This work provides a new approach for the synthesis of bio-based potassium sorbate in a food grade solvent. Previously we have done this reaction in a solvent that was not food safe. We also report higher potassium sorbate yields than we have previously reported.

2. We quantified our LCA greenhouse gas emissions for this process as 13.7 [9.6−18.6] kg CO_2-eq·kg^{-1} and estimated the economics of the technology.

3. Improvements in both (1) the yield and titer of biological TAL production and (2) the catalyst turnover frequency, along with lowering the reaction temperature, would significantly enhance the process and make this work greener in the future.

Sustainable Potassium Sorbate Production from Triacetic Acid Lactone in Food-grade Solvents

Min Soo Kim[1,2], Sarang S. Bhagwat[2,3], Leoncio Santiago-Martínez[1,2], Xiaolei Shi[1], Kyuhyeok Choi[1], Jeremy S. Guest[2,3], and George W. Huber[1,2]*

[1]Department of Chemical and Biological Engineering, University of Wisconsin-Madison, 1415 Engineering Drive, Madison, WI 53706, USA

[2]DOE Center for Advanced Bioenergy and Bioproducts Innovation (CABBI), University of Illinois Urbana-Champaign, 1206 W. Gregory Drive, Urbana, IL 61801, USA

[3]Department of Civil and Environmental Engineering, University of Illinois Urbana-Champaign, 3221 Newmark Civil Engineering Laboratory, 205 N. Mathews Avenue, Urbana, IL 61801, USA

*Corresponding author; email: gwhuber@wisc.edu

Abstract

This study advances the production of potassium sorbate (KS) from triacetic acid lactone (TAL) utilizing food-grade solvents, ethanol (EtOH) and isopropyl alcohol (IPA). We have previously demonstrated the route to produce KS from TAL in tetrahydrofuran (THF) as the main solvent, but the use of THF is associated with environmental and health risks especially for food applications. The process employs a catalytic approach in food-grade solvents and includes three main steps: hydrogenation, etherification and hydrolysis, and ring-opening hydrolysis to produce KS from TAL. In the synthesis of KS from TAL, the use of IPA leads to higher yields and reduced reaction times compared to EtOH. As a result, the overall reaction time in IPA was reduced to 35.7 hours, compared to 42.1 hours in our previous study using THF and EtOH, while achieving a comparable KS yield of 84% from TAL. The synthesized KS exhibits a *trans*-2, *trans*-4 geometrical configuration, identical to that of commercially available KS. Through techno-economic analysis (TEA) and life cycle assessment (LCA), we estimated full-scale production of KS from sugarcane with the developed process in IPA could achieve a minimum product selling price (MPSP) of \$8.27·kg^{-1} with a range of \$7.06−10.16·kg^{-1} [5th-95th percentiles from 6000 Monte Carlo simulations] and a carbon intensity (CI) of 13.7 [9.6−18.6] kg CO_2-eq·kg^{-1}. This study highlights the synthesis of KS from TAL using food-grade solvents, demonstrating improved economic viability and environmental sustainability compared to our previous research (MPSP of \$9.68·kg^{-1} [\$8.47−11.45·kg^{-1}] and CI of 16.2 [12.0−21.2] kg CO_2-eq·kg^{-1}, as the total required reaction decreases while achieving the comparable overall yield of KS from TAL.

Introduction

Environmental concerns, particularly related to rising carbon dioxide emissions and the increased reliance on nonrenewable fossil fuels, have led to a surge in research focused on sustainable ways to produce fuels and chemicals. As the abundant component of biomass, carbohydrates present themselves as viable feedstocks for creating renewable and eco-friendly chemicals derived from biomass.[1, 2] In contrast to fossil-based feedstocks, carbohydrates are abundant in oxygenated functional groups. This abundance is beneficial for synthesizing basic chemical building blocks, as it eliminates the need for hazardous and costly oxidative processes often required in upgrading carbohydrates into functional platforms or commodity chemicals.[3, 4]

4-hydroxy-6-methyl-2-pyrone, also known as triacetic acid lactone (TAL), is a biomass-based platform chemical that can be produced from lignocellulosic biomass through genetically modified polyketide biosynthesis pathways.[5-8] TAL can be converted into a range of commercial products and a variety of value-added chemicals.[9-12] Among the proposed valuable products, sorbic acid and its salt, potassium sorbate (KS), are widely utilized in the food and pharmaceutical industries as antimicrobial preservatives.[13, 14] KS is more commonly used because of its higher solubility in water, with 58.5 g of KS dissolving per 100 mL of water at room temperature, compared to 0.15 g for sorbic acid.[15-17] However, converting sorbic acid into its potassium salt form involves additional steps. Dumesic et al. proposed for the first time a catalytic conversion of TAL into sorbic acid.[10] Building on this, our team recently demonstrated a catalytic method for the synthesis of KS from TAL rather than making sorbic acid as an intermediate.[18] Fig. 1B illustrates the previous approach for producing TAL-derived KS. The process began with the hydrogenation of TAL in tetrahydrofuran (THF) to produce 4-hydroxy-6-methyltetrahydro-2-pyrone (HMP). After catalyst filtration, HMP underwent a dehydration reaction to yield parasorbic acid (PSA). Following the removal of THF, the isolated PSA with potassium hydroxide (KOH) was converted into KS through hydrolysis and ring-opening reactions in ethanol (EtOH).

Unfortunately, the KS that we produced is not food-grade because we used THF as the primary solvent.[19] The Food and Drug Administration (FDA) has issued a list of substances including solvents, categorized as secondary direct food additives that can be used in food

processing, subject to specific conditions outlined in Title 21 of the Code of Federal Regulations (CFR), Part 173-Subpart C.[20] THF is not an approved solvent for food additives. THF also has other health and safety concerns such as flammability, explosivity, and toxicity.[21-23] Prolonged exposure to THF may lead to a range of health issues, such as throat irritation, coughing, dizziness, and headaches. Inhalation is particularly concerning, as it has been linked to central nervous and respiratory irritation, with some evidence suggesting a potential carcinogenic impact.[24, 25]

To this end we should develop an improved approach to produce food-grade KS with a green solvent.[26, 27] Various studies have been undertaken to employ green solvents, aiming to replace hazardous counterparts and achieve efficient and sustainable development.[28-30] Capello et al.[26] evaluated 26 commonly used solvents on their environmental impact through their life cycle, identifying simple alcohols, and alkanes such as hexane and heptane, as environmentally preferable. In contrast, the utilization of acetonitrile, formaldehyde, and THF was deemed unfavorable due to environmental concerns. Beyond the environmental considerations, isopropyl alcohol (IPA) and EtOH, which are generally considered as green solvents, show more energy-efficient in their production compared to THF. Specifically, THF production requires a cumulative energy demand (CED) of 270.8 MJ-eq per kg of solvent, while EtOH and IPA necessitate 50.1 and 65.6 MJ-eq per kg of solvent, respectively. This emphasizes the broader advantages of transitioning to these environmentally friendly solvents, not only in terms of safety but also for energy efficiency. Both EtOH and IPA are approved for use as processing solvents in the food industry. EtOH is recognized by FDA as Generally Recognized as Safe (GRAS) for specific uses, including as an antimicrobial agent on pizza crusts prior to final baking, up to 2% by weight.[31] Isopropyl alcohol, while not GRAS for direct food use, is permitted for specific uses in food production, with allowable residue levels ranging from 6 ppm to 2% by weight depending on the particular use.[32] Additionally, IPA is permitted to be used as a sanitizer on food-processing equipment and utensils, as well as food-contact surfaces.[33] This demonstrates the versatility and regulatory acceptance of these solvents in food-related applications.

In this paper, we propose a sustainable route to produce food-grade TAL-derived potassium sorbate (TAL-KS) utilizing green solvents such as EtOH and IPA, as depicted in Fig. 1A. This approach achieves an overall yield comparable to that of our previous study while reducing

the reaction time required and avoiding the use of THF. Interestingly, the TAL-KS synthesized in IPA exhibits a *trans*-2, *trans*-4 geometrical configuration, identical to commercial KS, whereas our previous study observed that the TAL-KS produced in EtOH had a *cis*-2, *trans*-4 configuration. Further investigation into the *cis*-2, *trans*-4 KS concerning a safety aspect is necessitated since distinct properties of compound isomers could influence safety profiles, leading to unforeseen side effects[34-37] (despite showing antimicrobial activities comparable to those of commercial KS[18]). Further, we characterized the minimum product selling price (MPSP) via techno-economic analysis (TEA) and carbon intensity (CI) via life cycle assessment (LCA) of biorefineries leveraging the developed catalytic upgrading technologies to produce KS from sugarcane (following design and evaluation assumptions for sugarcane-to-TAL biorefineries in our previous study[38]). To better understand the economic and environmental implications of the process improvements achieved in this work as well as potential future improvements, we designed and simulated biorefineries across the theoretical catalytic upgrading space (i.e., across possible combinations of product yields and reaction times for hydrogenation, etherification and hydrolysis, and ring-opening and hydrolysis). Finally, we explored research and development opportunities along the value chain (e.g., in the microbial conversion of sugars to TAL, TAL separation, multiple-feedstock processing) to advance the financial viability and environmental sustainability of bio-based KS production.

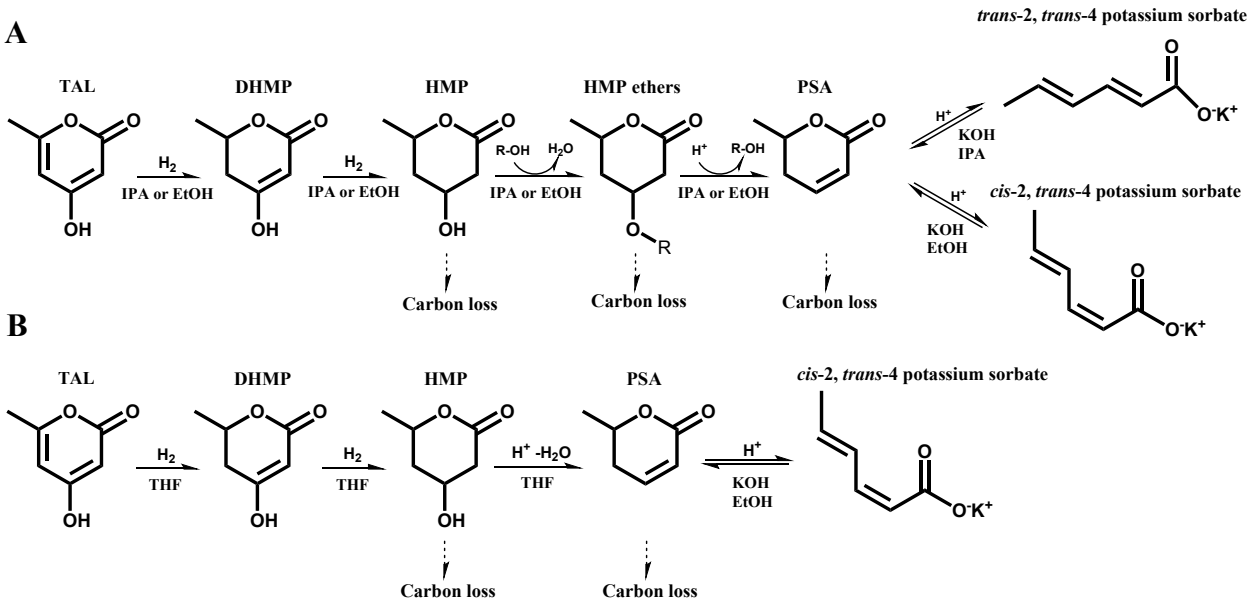

Fig. 1. Reaction pathways for producing TAL-derived potassium sorbate in (A) EtOH or IPA and (B) THF and EtOH [18]. Compounds are as follows: tetrahydrofuran (THF); ethanol (EtOH); 2-propanol (IPA); 4-hydroxy-6-methyl-2-pyrone/triacetic acid lactone (TAL); 5,6-dihydro-4-hydroxy-6-methyl-2*H*-pyran-2-one (DHMP); 4-hydroxy-6-methyltetrahydro-2-pyrone (HMP); 6-methyl-5,6-dihydro-2-pyrone/parasorbic acid (PSA).

Experimental methods

Materials

The chemicals used in this work were purchased or synthesized as follows: Triacetic acid lactone 98% (TAL, Oakwood Chemical), 5,6-dihydro-4-hydroxy-6-methyl-2H-pyran-2-one 98% (DHMP, Sigma Aldrich), δ-hexalactone 98% (DHL, Sigma Aldrich), Ethanol 200 (EtOH, Decon labs inc.), Isopropyl alcohol (IPA, Sigma Aldrich), Tetrahydrofuran (THF, Alfa Aesar, trans,trans-2,4-Hexadienoic acid potassium salt (potassium sorbate, KS, AmBeed), Potassium hydroxide powder (KOH, Sigma Aldrich). Water with 0.1% formic acid (HPLC grade, Fisher Scientific), Acetonitrile (HPLC grade, Sigma Aldrich), Tetraamminepalladium nitrate (10 wt% in water, Sigma Aldrich). The commercial catalysts used in this work were purchased as follows: 65 wt% nickel on silica (Ni/SiO_2, STREM), 65 wt% nickel on silica-alumina (Ni/Si-Al, Sigma Aldrich), Amberlyst™ 70 (Amberlyst 70, Rohm and Haas). Dimethyl sulfone ($DMSO_2$, Sigma Aldrich), Deuterium oxide (D_2O, Sigma Aldrich), Chloroform-d ($CDCl_3$, Sigma Aldrich). Catalytic reactions were performed in Parr reactor (Parr Instrument Company).

Catalyst synthesis and characterization

2 wt% Pd/Al_2O_3 (Pd/Al_2O_3) catalyst was synthesized by incipient wetness impregnation of a 10 wt% $Pd(NH_3)_4(NO_3)_2$ solution in water. The catalyst was dried for >12 h at 100°C with air in an oven. The dried catalyst was calcined at 500°C in 100 mL/min air flow (3°C min^{-1} ramp, 4 h hold), reduced at 300°C in 100 mL/min H_2 flow (3°C min^{-1} ramp, 4 h hold), then passivated at room temperature with 30 mL/min 1% O_2/Ar flow in a glass tube reactor. The commercial Ni catalysts (Ni/Si-Al and Ni/SiO_2) were pre-reduced at 400°C in 100 mL/min H_2 flow (3°C min^{-1} ramp, 4 h hold), then passivated at room temperature with 30 mL/min 1% O_2/Ar flow for 3 h in a glass tube reactor.

The CO chemisorption studies were carried out using a Micromeritics Autochem II 2920. The 130 mg of Pd catalyst and 50 mg Ni catalysts were *in situ* reduced under H_2 flow at 300°C and 400°C, respectively. After reduction, CO adsorption was performed at 35°C by pulse chemisorption of 10% CO/He. The adsorption stoichiometry between CO and surface Pd or Ni sites was assumed to be 1:1. CO chemisorption was used to estimate the number of Pd or Ni metallic sites (Table S1 in ESI).

Product analysis and quantification

4-hydroxy-6-methyltetrahyro-2-pyrone (HMP), parasorbic acid (PSA), ethoxy-HMP (EHMP), and isopropoxy-HMP (IHMP) are not commercially available, thus these compounds were synthesized from TAL. ^{1}H NMR and ^{13}C NMR were used to identify those compounds. The detailed description of the synthesis processes can be found in the subsection titled "Batch reactor studies".

GC-FID analysis

The Shimadzu gas chromatograph (GC) equipped with a flame ionization detector was used to analyze HMP, DHMP, DHL, IHMP, EHMP, and PSA. The Restek RTX-VMS capillary column used had a length of 30 meters, an inner diameter of 0.25 mm, and a film thickness of 0.25 µm. The injection port and FID were maintained at a temperature of 240°C. The sample injection volume was 1 µL, and a split ratio of 50 was employed. The column temperature ramp followed this sequence: hold the temperature at 40°C for 1 min, then ramp up at a rate of 10°C min^{-1} to 180°C, followed by a slower ramp of 3°C min^{-1} to 240°C. The temperature was held constant at 240°C for 5 min.

HPLC analysis

TAL was quantified by reversed-phase high-performance liquid chromatography (HPLC) with a Luna C18(2) column (Phenomenex Inc., part no. 00G-4252-E0) for separations conducted at 50°C and a Waters 2998 PDA detector set to 325 nm for TAL. The solvent gradient was followed elution profile: Solvent A, 1%(v/v) formic acid in water; Solvent B, acetonitrile; Gradient: 2% B to 7% B (linear gradient, 0-5 min), 7% to 95% B (5-10 min), 95% B (isocratic elution 10-13 min), 95%

B to 2% B (13-15 min), 2% B (isocratic elution. 15-17 min); flow rate 1.0 mL/min. All samples were filtered with a 0.2 μm PTFE syringe filter prior to analysis.

NMR analysis

Nuclear magnetic resonance (NMR) was obtained using a Bruker Avance-400 spectrometer. ^{1}H NMR and ^{13}C NMR spectra were employed to identify compounds synthesized such as HMP, PSA, IHMP, and EHMP. Additionally, NMR was used for analyzing the geometric configurations of commercial KS and produced KS. Deuterated solvents and dimethyl sulfone (internal standard) were used as references.

Batch reactor studies

The reactions involving TAL and HMP with catalysts (Pd/Al_2O_3, Ni/Si-Al, and Ni/SiO_2) were conducted in either a 45 mL or 75 mL Parr reactor. The catalysts employed in the TAL hydrogenation were pre-treated to be reduced and passivated. Moreover, to load the catalysts in a glove box, the Pd/Al_2O_3 catalyst underwent calcination at 500°C in a 100 mL/min air flow (with a ramp rate of 3°C min^{-1} and 4 hours hold), followed by reduction at 300°C for the Pd catalyst and at 400°C for the Ni catalyst using a 100 mL/min hydrogen flow (with a ramp rate of 3°C min^{-1} and 4 hours hold) in a glass tube reactor equipped with ball valves at the inlet and outlet. After cooling to room temperature and stopping the H_2 flow, the ball valves were closed, and the catalyst was transferred to the glove box with a positive-pressure N_2 atmosphere for storage.

Before the TAL hydrogenation process, the reduced catalyst and a magnetic stir bar were introduced into a 45 mL Parr reactor within the glove box. Following the closing of the Parr reactor and removal of the Parr reactor from the glove box, the Parr reactor was pressurized with 10 bar H_2. Subsequently, a TAL solution was fed into the Parr reactor using an HPLC pump to prevent exposure to air. The Parr reactor contained the TAL solution and the catalyst with the magnetic stir bar, ensuring continuous stirring of the reaction mixture at 750 rpm. The Parr reactor underwent three purges with 30 bar Ar, followed by pressurization to 30 bar of H_2, and then heating to 100°C. Reactions of HMP with Amberlyst 70 and PSA with KOH were also carried out in the 45 mL Parr reactor. For these reactions, the reactor was purged three times with 30

bar Ar, followed by pressurization to 30 bar Ar, and then heating to the desired temperatures. The heat-up time was in the range of 15-20 mins. The reaction time was recorded once the reactors reached the desired reaction temperature. Following completion of the reaction, the products from TAL and HMP were cooled to room temperature using an ice bath, and filtered with a 0.22 μm PTFE syringe filter before being injected into the GC-FID. To obtain a product solution over different time intervals, 1 mL samples were collected by inserting a dip tube into the Parr reactor. Each product solution was filtered with a 0.22 μm PTFE syringe filter before being injected into the GC-FID. The detail synthesis and analysis of products from PSA were provided in the *KS synthesis* section.

Isolated HMP, PSA, EHMP, and IHMP production

The detailed synthesis process for producing HMP and PSA was described in our previous work.[18] To synthesize HMP, 2 g of TAL was dissolved in 40 mL of THF in a 75 mL Parr reactor with a stir bar at 750 rpm and 0.5 g of Pd/Al_2O_3 to prevent the formation of IHMP or EHMP. The Parr reactor was sealed and purged 3 times with 30 bar Ar. Then, the Parr reactor was pressurized at 70 bar H_2. The temperature was kept at 100°C for the duration of the synthesis which was 24 hours. The heat-up time was in the range of 15-20 mins. After the reaction, the product solution was cooled to room temperature using an ice bath, filtered with a 0.22 μm PTFE syringe, and then the HMP product solution was confirmed in GC-FID and NMR. The HMP solution product was isolated using a rotary evaporator, with the sample heated in an oil bath controlled at 40°C and 50 mbar. To synthesize EHMP or IHMP, 1 g of the isolated HMP was dissolved in 40 mL of EtOH or IPA in the 75 mL Parr reactor with stir bar at 750 rpm and 0.5 g of Amberlyst 70, HMP/Cat=2:1. The temperature was kept at 70°C for 18 hours for both the EHMP and IHMP synthesis. To synthesize PSA, 1 g of the isolated HMP was dissolved in 40 mL of THF in the 75 mL Parr reactor with stir bar at 750 rpm and 0.5 g of Amberlyst 70, HMP/Cat=2:1. The temperature was kept at 140°C for 12 hours. The products (EHMP, IHMP, and PSA) were isolated in the same manner as for the HMP isolation described above. The products were analyzed by ^{13}C NMR and ^{1}H NMR (Fig. S3-S5 in ESI). The synthesized HMP, PSA, IHMP, and EHMP were used as the calibration standard for the GC analysis.

KS synthesis

To ensure accurate purity of PSA, the PSA feed was measured in ^{1}H NMR with $DMSO_2$ as an internal standard. In the ^{1}H NMR spectra, when the purity of PSA is 100%, the anticipated integrated area ratio of $DMSO_2$ (6H) to PSA (1H) is expected to be six. In this study, a purity of 88% was measured, as shown in Fig. S3. An equivalent molar amount of KOH (0.5 g, 0.84 mmol) was added to an 87.9% purity of the isolated PSA (0.11 g, 0.84 mmol) dissolved in 20 mL IPA in a 45 mL Parr reactor. The Parr reactor was purged three times with 30 bar Ar, and pressurized to the reaction pressures, then heated to 130°C. The heat-up time was in the range of 15-20 mins. After the reaction, the KS product solution was cooled to room temperature using an ice bath. The precipitated KS was separated using a vacuum filtered by paper while rinsing with ~50 mL IPA. Besides, the solvent containing the dissolved KS in IPA was loaded in a 40 mL glass vial, then removal of the solvent was conducted using a rotary evaporator in an oil bath controlled at 40°C and 50 mbar. The precipitated KS and isolated KS in the glass vial were further dried in a vacuum oven at 50°C under 500 mbar for 12 hours. Finally, a yield of each sample was measured by ^{1}H NMR by adding the equivalent molar amount of $DMSO_2$ (0.84 mmol).

Reaction kinetic modeling

Experimental data were collected by inserting a dip tube into a Parr reactor, and these results were compared to a proposed kinetic model for the conversion of HMP to PSA. The kinetic model comprised a set of interconnected nonlinear ordinary differential equations, and the rate constants were determined using the Arrhenius equation, which accounts for the temperature-dependent nature of the reaction. Concentration data of reactants and products at various temperatures were utilized to numerically adjust the rate parameters of the reaction equations. To obtain the rate parameters for both IHMP and PSA decomposition over Amberlyst 70, experiments were conducted using 40 mM PSA in IPA as the feedstock. 25 mL of the 40 mM PSA in IPA with 0.06 g of Amberlyst 70 was loaded in the 45 mL Parr reactor with a stir bar at 750 rpm. The Parr reactor was sealed and purged 3 times with 30 bar Ar. Then, the Parr reactor was pressurized at 30 bar Ar. The temperature was kept at 100, 130, and 160°C. The heat-up time was in the range of 15-20 mins. The reaction time was recorded once the reactors reached the

desired reaction temperature. 1 mL of samples was obtained by inserting a dip tube into the Parr reactor over different reaction times. Each product solutions were filtered with a 0.22 μm PTFE syringe filter before being injected into the GC-FID.

It was assumed that the concentration of reactants did not significantly influence the decomposition products. MATLAB ODE 45 function (R2020b) was employed to numerically integrate the ordinary differential equations and estimate the kinetic parameters, employing the lsqnonlin function. Subsequently, the nplarci function in MATLAB was utilized to perform an error analysis of the regressed data and calculate the 95% confidence interval for each rate constant, utilizing residual and Jacobian matrices. The estimated rate constants were then used in an Arrhenius equation, and the pre-exponential factors and activation energies were simultaneously determined using the LINEST function in Excel, which employs a least-squares method.

Biorefinery design, simulation, techno-economic analysis, and life cycle assessment

Biorefinery design and simulation

The biorefinery was designed, simulated, and evaluated using BioSTEAM[39, 40] and the thermodynamic package utilized was Thermosteam[41, 42]. Briefly, influent and effluent streams of each unit are simulated in BioSTEAM and coupled with operating parameters and equipment cost algorithms for unit design and cost calculations. Component equipment for major units (Table S4 in ESI) as well as baseline values and uncertainty distributions of key parameters (Table S5 in ESI) are included in the Supplementary Material. All Python scripts for BioSTEAM and the biorefinery (including biorefinery setup and system analyses) as well as a system report (including detailed process flowsheet, stream composition and cost tables, unit design specifications, and utilities for the baseline simulation) are available in the online repository.[43] The biorefineries in this study are comprised of four main (inside battery limits) processes (feedstock juicing and clarification, fermentation, separation, and catalytic upgrading) with outside-battery wastewater treatment and miscellaneous facilities (boiler, turbogenerator, cooling utility regeneration, heat exchanger network, clean-in-place, air distribution, fire water distribution, and process water distribution) with all design assumptions (other than for catalytic upgrading) consistent with Bhagwat et al.[38]. The biorefinery's production capacity was 15,940 metric ton KS·y^{-1} in the baseline case, which is

equivalent to 11,900 metric tons of sorbic acid annually assuming theoretical maximum conversion. This production capacity was chosen based on (i) the growth projected in the annual U.S. demand for sorbic acid between 2020–2030 (from approximately 23,800 metric tons of sorbic acid in 2019 to a projected 34,550 metric tons of sorbic acid in 2030) and (ii) the amount by which the 2019 U.S. consumption of sorbic acid (23,800 metric tons) exceeded the 2019 U.S. production capacity (12,375 metric ton·y^{-1}).[44] This translates to a baseline biorefinery accepting 653,160 metric ton·y^{-1} of sugarcane; this is well within the reported annual capacity for an intermediate-size sugarcane processing facility (1,600,000 metric tons[45]) that has been assumed in previous sugarcane biorefinery TEAs.[46-48] The biorefinery was assumed to operate 180 days annually in the baseline case based on typical sugarcane harvesting periods.[46-48] Assumptions related to feedstock composition (Table S3 in ESI), as well as baseline values and distributions for all parameters included in the uncertainty analysis (Table S5 in ESI), are detailed in the Supplementary Material.

Techno-economic analysis (TEA)

We performed TEA for the designed and simulated biorefineries using BioSTEAM's discounted cash flow rate of return analysis to calculate the minimum product selling price (MPSP, \$·kg^{-1}) of KS to achieve a net present value of zero with a 10% annual internal rate of return (a uniform distribution of 8−12% was assumed to be consistent with Bhagwat et al.[38]; a full list of baseline parameter values, uncertainty distributions, and literature references for the same are provided in Table S5 in ESI). All costs and prices shown are presented in 2019 U.S. dollars. To benchmark the MPSP of the produced KS, we assumed a market price range of \$5.03−6.50·kg^{-1} based on a 2023 vendor listing for the high end (6.50·kg^{-1}) and a market report for the low end (6.74·kg^{-1} sorbic acid in 2019, equivalent to \$5.03·kg^{-1} KS conservatively assuming 100% conversion).[44, 49] The biorefinery was modeled as an n^{th} plant design (i.e., it is assumed a successful industry has been established with mature technologies). We assumed the industrial-scale technological performance of the developed catalytic upgrading process would reflect the reaction times, catalyst loading and conversions achieved at the bench scale in this study. To evaluate the implications of uncertainty in the industrial-scale technological performance of the developed catalytic upgrading process, we attributed large uncertainties to the reaction times,

catalyst loading and conversions of the hydrogenation, etherification and hydrolysis, and ring-opening and hydrolysis reactors, and further evaluated the sensitivity of system cost and environmental impacts to these parameters (uncertainty and sensitivity analyses described further in the *Uncertainty and Sensitivity Analyses* section; full lists of the evaluated parameters, their uncertainty distributions, and literature references are provided in Tables S5 and S6). Key construction (e.g., warehouse, site development), fixed operating (e.g., labor burden, property insurance), and financial (e.g., depreciation, taxes) parameters, as well as all parameters used in the cash flow analysis, followed assumptions made by Bhagwat et al.[38]. A breakdown of the estimated revenue and capital and operating expenditures, as well as additional details on the design, utility requirements, purchase costs, and installed equipment costs can be found online.

Life cycle assessment (LCA)

We performed LCA in Python using the simulated inventories for streams (input chemicals and output emissions) and utilities from BioSTEAM. The LCA scope included the operational phase of the biorefinery, including cradle-to-grave impacts for all raw materials, ancillary processes, and unit processes. The functional unit was set to 1 kg of produced KS to be consistent with the TEA. The sale of co-produced electricity was assumed to displace the impacts of marginal electricity production. Impacts resulting from infrastructure construction were excluded to be consistent with the U.S. renewable fuel standard (RFS).[50] Final characterization and discussion of environmental impacts focused on carbon intensity (CI; quantified as 100-year global warming potential, GWP_{100}). The impact assessment methodology used for CI was Intergovernmental Panel on Climate Change (IPCC) 2013.[51] Life cycle inventory data were collected from ecoinvent 3.8 and some unit impacts were gathered from GREET 2020[52, 53], and their sources were noted in the script[43]. The baseline impacts of feedstock farming (excluding credit for fixed carbon), harvest and collection, transportation, storage, and handling were considered (Table S5 in ESI). The amount of carbon fixed in the feedstock is equal to the sum of carbon in the product (KS) and in the biogenic portion of direct waste emissions from the biorefinery. To focus on the biorefinery, we assumed the end-of-life impacts associated with the product (KS) as well as non-gaseous wastes (e.g., unconsumed and non-combusted sugars and insoluble lignin in the brine, accounting for <0.05% of the CI) would be exclusively from the oxidation of all carbon into CO_2.

Uncertainty and Sensitivity Analyses

Uncertainty analyses were conducted using Monte Carlo simulation with Latin Hypercube Sampling (6,000 simulations) for 50 uncertain parameters in the *THF & EtOH*, *IPA*, and *catalysis improv.* scenarios, and for 51 parameters in the *all-round improv.* scenario. We assigned uncertainty distributions for parameters to be consistent with Bhagwat et al.[38], except for the parameters describing the catalytic upgrading processes developed in this work, for which uniform distributions of ±10% of the baseline were assumed. The full list of the evaluated parameters, their uncertainty distributions, and literature references are provided in Tables S5 and S6. The sensitivity of MPSP and CI to all uncertain inputs was determined via Spearman's rank order correlation coefficients (Spearman's ρ) using Monte Carlo simulation results, and only parameters with |Spearman's ρ| ≥ 0.10 and p-value < 0.05 were discussed to ensure robustness. In addition, the improvements in sustainability indicators in response to technological advancements in catalytic upgrading, fermentation, separation, and integrated sweet sorghum processing were also characterized. For catalytic upgrading, indicator sensitivity to product yields (mol%) and reaction times (h) for hydrogenation, etherification and hydrolysis, and ring-opening and hydrolysis reactors were for batch and continuous mode operation. System sustainability for potential scenarios with improved catalytic upgrading, fermentation (increased TAL yield and titer), separation (decreased TAL loss by ring-opening decarboxylation with pH control by base addition), and sweet sorghum integration (increasing the biorefinery's annual operating time) were also characterized by uncertainty analyses with 6000 Monte Carlo simulations in each scenario (full lists of the evaluated parameters, their uncertainty distributions, and literature references are provided in Tables S5 and S6). Files with comprehensive results of all analyses are available online.[43]

Results and discussion

TAL hydrogenation to HMP

The hydrogenation of TAL was conducted with EtOH, IPA, and THF to investigate the influence of green solvents in the presence of three different catalysts: Pd/Al_2O_3, Ni/SiO_2, and Ni/Si-Al. In this study, two distinct catalyst pretreatment techniques were evaluated. First, the

catalysts underwent pretreatment of reduction, followed by passivation. Another pretreatment method was that after reduction the catalysts were transferred into the batch reactor within a glove box while avoiding exposure to air, followed by introducing the TAL solution into the reactor using an HPLC pump. As shown in Fig. 2, the catalyst reduction procedure had no effect on the catalyst activity or selectivity. We thus used the catalysts pretreated by reduction and passivation in future sections of this paper. The CO uptake and dispersion of Pd and Ni catalysts employed are summarized in Table S1 in ESI. The turnover frequency (TOF) was calculated using the following equation:

$$TOF\ (min^{-1}) = \frac{Inital\ HMP\ production\ rate\ (\mu mol/g_{cat}/min)}{CO\ uptake\ (\mu mol/g_{cat})} \quad (1)$$

Fig. 2 shows the TOF and 4-hydroxy-6-methyltetrahydro-2-pyrone (HMP) selectivity for TAL hydrogenation in different solvents. The TOF with the Pd/Al_2O_3 catalyst was similar with all solvents ranging from 2.59 min^{-1} in EtOH, 3.19 min^{-1} in IPA, and 3.24 min^{-1} in THF. Conversely, the TOF varied with Ni/Si-Al from 0.54 min^{-1} in ETOH to 0.78 min^{-1} in THF.

In THF, a high overall selectivity for HMP was observed; however, the HMP selectivity was comparatively lower in EtOH and IPA when using Pd/Al_2O_3. A higher HMP selectivity was obtained over the Ni-based catalysts across the solvents, aligning with our previous study due to the formation of δ-hexalactone (DHL).[18] A negligible amount of DHL was produced over the Ni-based catalysts. However, the catalyst pretreatment conducted in this study resulted in less DHL formation than in our previous study. The main byproducts formed were the ethers with ethoxy-HMP (EHMP) forming in EtOH and isopropoxy-HMP (IHMP) forming in IPA. No ethers were formed in THF. Multiple reaction points were taken with the Ni/Si-Al to understand this catalyst in more detail, as shown in Fig. 3. As the reaction time increased the HMP-ether increased. The formation of EHMP was preferred than that of IHMP, aligning with the expected reactivity of primary alcohols and consistent findings from previous research.[54, 55] The following section shows the conversion of HMP and HMP ethers into PSA.

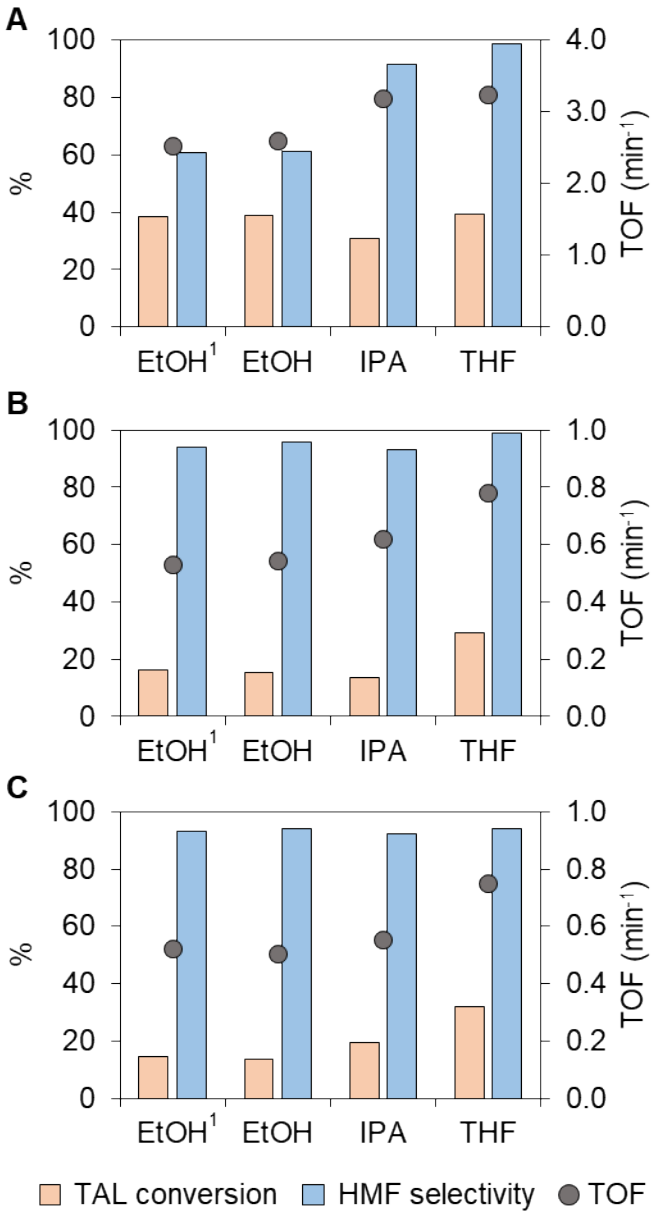

Fig. 2. Catalytic performance for the production of HMP from TAL in different solvents over (A) Pd/Al_2O_3, (B) Ni/Si-Al, and (C) Ni/SiO_2. Reaction conditions: batch reactor, TAL (38.9-40.2 mM) in 25 mL of solvent, Mass ratio catalyst: TAL = 1:5, 100°C and 30 bar H_2. TOF measured at HMF conversions below 40%, achieved by varying the reaction time. [1]After reduction, the catalyst was loaded to the batch reactor within a glove box, and the HMP solution was fed to the reactor via the HPLC pump.

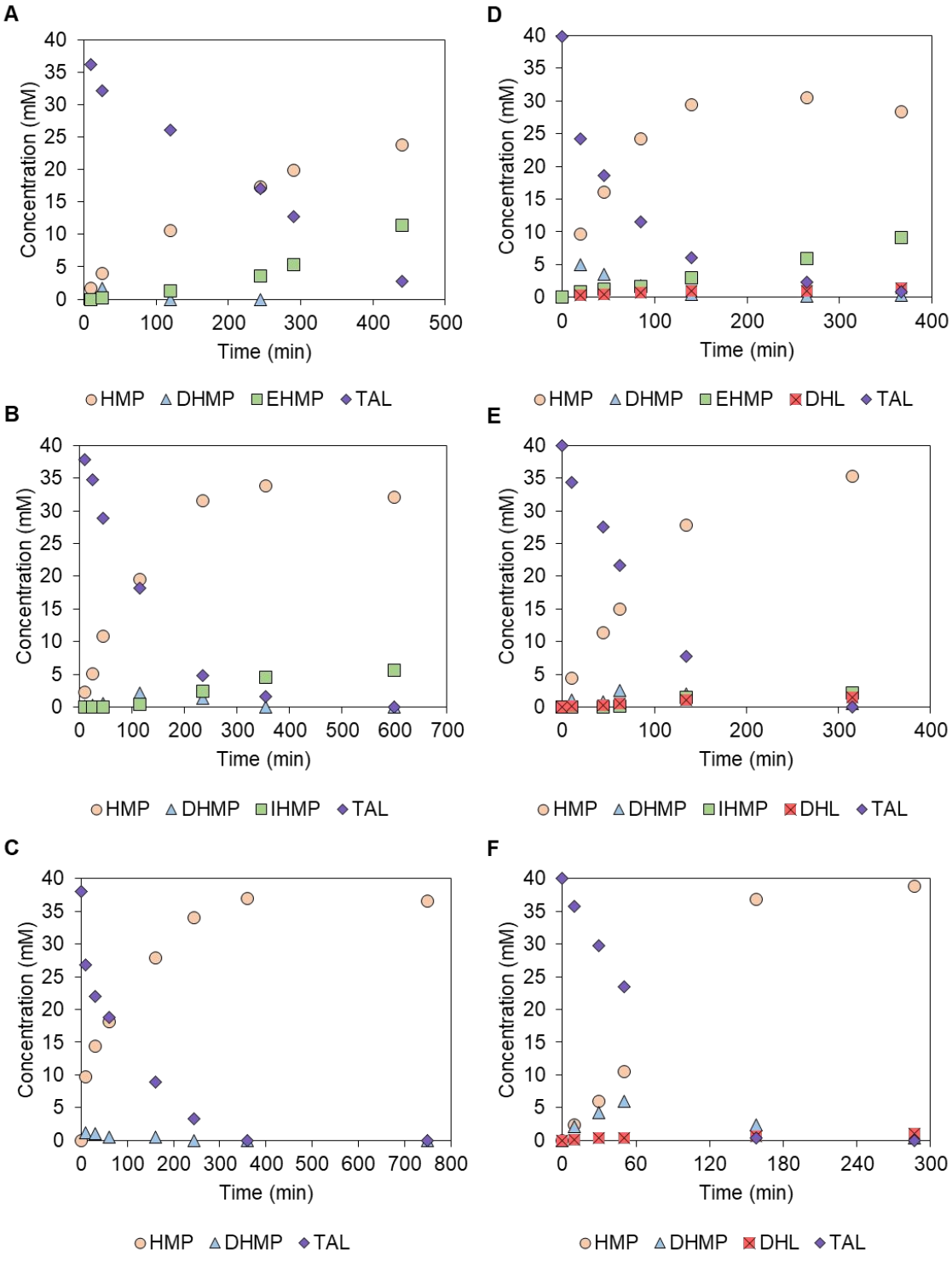

Fig. 3. TAL hydrogenation over Ni/Si-Al in (A) EtOH, (B) IPA, and (C) THF; over Pd/Al_2O_3 in (D) EtOH, (E) IPA, and (F) THF. Reaction conditions: batch reactor, TAL (38.2-39.8 mM) in 25 mL of solvent, Mass ratio catalyst: TAL = 1:5, 100°C, 30 bar H_2.

PSA production from HMP

The conversion of HMP to PSA was studied using Amberlyst 70 with three solvents: EtOH, IPA, and THF. The HMP-ethers, such as ethoxy-HMP (EHMP) and 2-propoxy HMP (IHMP), were formed in EtOH and IPA, respectively. No products from self-etherification of EtOH and IPA were detected. Fig. 4 presents the data on HMP conversion to PSA and its ethers, alongside the carbon balance. The carbon balance was calculated by subtracting the outputs of PSA, HMP ethers, and remaining HMP from the initial HMP input. The use of THF led to a 98% conversion of HMP, achieving a PSA selectivity of 99% and a carbon balance of 77%. In IPA, the conversion was 94%, with a carbon balance of 86.9%, and a PSA and IHMP selectivity of 69% and 31%, respectively. Meanwhile, EtOH resulted in an 82% conversion with an 85% carbon balance, yielding a selectivity of 59% for PSA and 41% for EHMP. The order for HMP conversion and PSA selectivity was as follows: EtOH < IPA < THF, whereas the order of the carbon balance was THF < EtOH < IPA.

Although IPA exhibits slightly lower conversion and PSA selectivity in comparison to THF, it has a higher carbon balance. This finding underscores the potential of IPA not only as a more food safe option but also as a viable alternative in the synthesis process. The previous research noted that a lower carbon balance occurred over increasing reaction times and elevating temperatures, attributed to the formation of decomposition products.[18] We thus performed a detailed investigation into the reaction kinetics of PSA production from HMP in IPA as described in the next section.

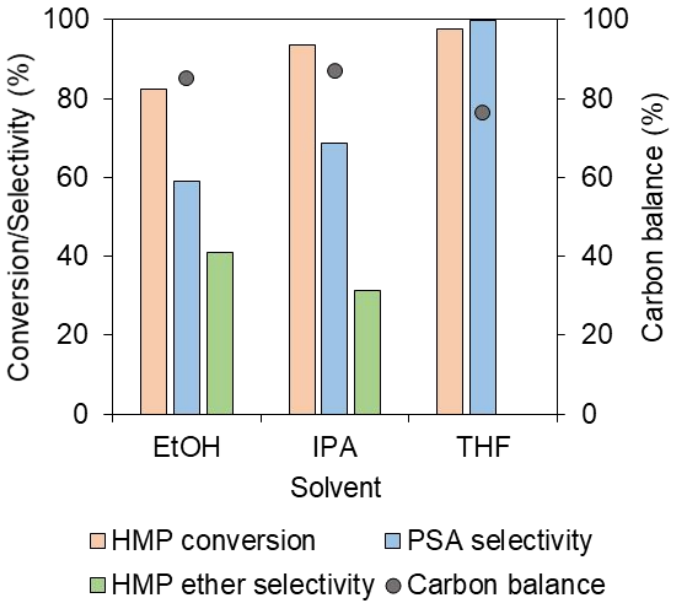

Fig. 4. HMP conversion over Amberlyst 70 in EtOH, IPA, and THF. Reaction conditions: batch reactor, HMP (40.5 mM) in 25 mL of solvent, Mass ratio catalyst: HMP = 1:2, 130°C and 30 bar Ar, 6.5 hours.

Reaction kinetics model for PSA production

The production of PSA from HMP was conducted in the temperature range of 100°C to 160°C in IPA with Amberlyst 70 to obtain a deeper understanding of the reaction mechanism. Consequently, kinetic analyses were performed to estimate the rate constants, enabling the determination of the optimal reaction conditions, including temperature and time. Scheme 1 depicts the proposed reaction mechanism for the production of PSA from HMP in IPA. The reactions were modeled as first-order and irreversible. Initially, HMP undergoes etherification to yield IHMP (Eqn. 2). This is succeeded by the hydrolysis of IHMP, which produces PSA and IPA (Eqn. 3), where it is assumed that the concentration of IPA does not significantly affect the production of PSA. The remaining reactions involve the formation of decomposition products from HMP, IHMP, and PSA (Eqn. 4-6).

$$HMP + IPA \xrightarrow[k_1]{} IHMP + H_2O \quad (2)$$

$$IHMP \xrightarrow[k_2]{} PSA + IPA \quad (3)$$

$$HMP \xrightarrow[k_3]{} D \quad (4)$$

$$IHMP \xrightarrow[k_4]{} D \quad (5)$$

$$PSA \xrightarrow[k_5]{} D \quad (6)$$

$D \equiv$ decomposition products

Scheme 1. Etherification, hydrolysis and decomposition formation during PSA production from HMP.

The rate expressions for HMP etherification, IHMP hydrolysis, and decomposition formations from HMP, IHMP, and PSA can be formulated as shown in Fig. 5E. The rate expressions were used to fit the kinetic data shown in Fig. 5A-C. PSA degradation experiment was conducted separately as a function of temperature and time to obtain the rate constant (k_5), as shown in Fig. S1 in ESI. The degradation rate was relatively slow and was observed to follow a first order decomposition. The kinetic parameters with the standard errors are reported in Table S2 in ESI. The activation energy for IHMP hydrolysis to PSA was calculated to be 74.4 kJ/mol which is the highest activation energy among the proposed reactions (Fig. 5D). The results indicated that the highest PSA yield occurs at high temperatures and short reaction times. Based on the kinetic parameters, the maximum PSA yield in IPA was computed to be 87% at 160°C with a reaction time of 367 min. The experimental PSA maximum yield at 160°C was 85% with the reaction time of 370 min. This contrasts with our previous study that showed that the maximum yield of PSA in THF occurs at a lower temperature and a longer reaction time. The maximum PSA yield in THF was 87% based on kinetic reactions study and experimentally achieved 84% at 100°C with the reaction time of 1,070 min.[18] In our study, the choice of solvent significantly impacts the reaction pathway for producing PSA from HMP over Amberlyst 70. Using IPA introduces IHMP as an intermediate, allowing for higher temperatures with less formation of decomposition products. This difference in mechanism between the solvents directly influences the reaction kinetics of the PSA production process.

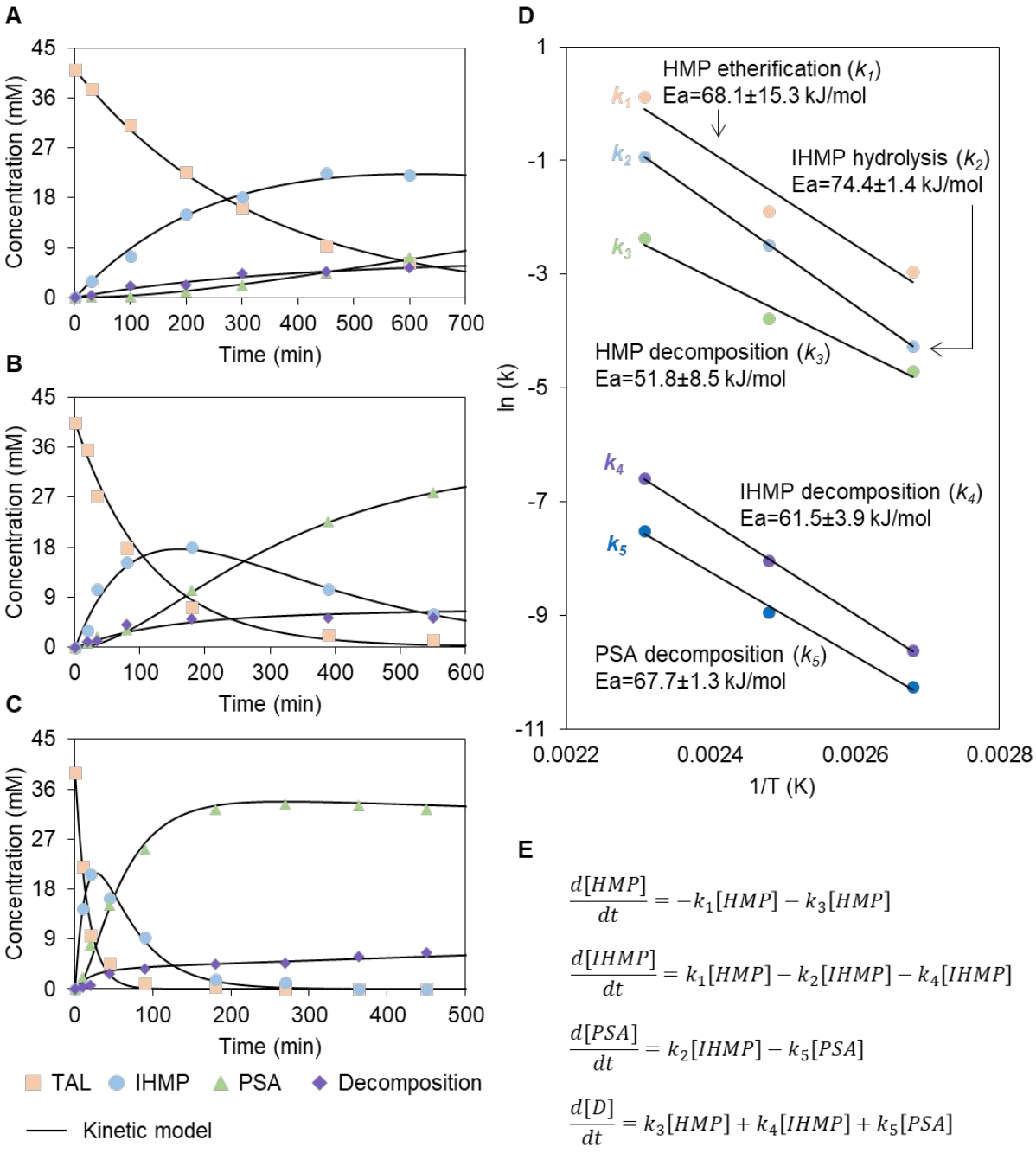

Fig. 5. Experimental data vs. kinetic model for PSA production from HMP in IPA over Amberlyst 70 at (A) 100°C, (B) 130°C, and (C) 160°C. Reaction conditions: batch reactor, HMP (39.0-41 mM) in 25 mL of IPA, Mass ratio catalyst: HMP = 1:2, 30 bar Ar. (D) Arrhenius plot of ln(k) vs. 1/T for PSA production from HMP over Amberlyst 70 in IPA. (E) The rate expressions for PSA production from HMP.

PSA ring-opening and hydrolysis to KS

Previous studies observed that the addition of H_2O as a co-solvent resulted in a lower reactivity of the hydrolysis process.[18, 56] Khurana et al.[56] investigated the role of solvent selection in optimizing the hydrolysis process using KOH. KOH has a solubility of 38.7 grams per 100 grams of EtOH, while its solubility in THF is negligible.[57] As a result, KS produced from PSA with KOH in EtOH exhibited a higher yield than in THF or a mixture of THF and H_2O. In this context, IPA was deemed an appropriate solvent for the ring-opening and hydrolysis reactions, given that 14g of KOH can dissolve in 100g of IPA. This study added equal moles of KOH as a co-reactant to produce PSA with an 88% purity (Fig. S3 in ESI) using IPA as a solvent.

KS was successfully produced from PSA in IPA over KOH. Fig. 6A shows that the KS yield increased with increasing reaction time, reaching >99% at 19 hours. The complete conversion of PSA into KS in EtOH was achieved in a shorter reaction time because of the higher solubility of KOH in EtOH than in IPA. The KS synthesized in IPA precipitated out because KS is not soluble in IPA, as shown in Fig. 6B.

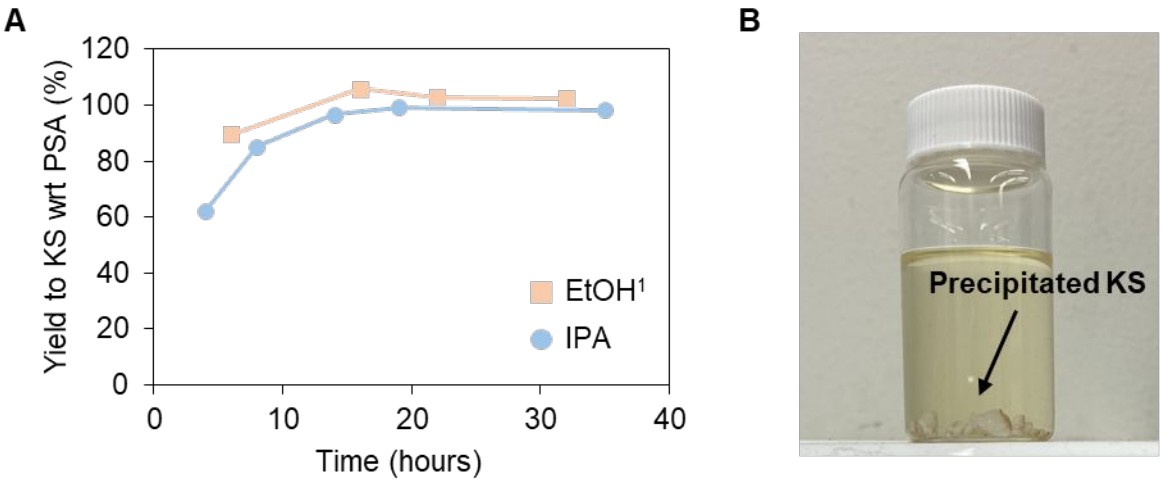

Fig. 6. (A) PSA conversion to KS in EtOH and IPA. Reaction condition: Batch reaction, 0.84 mmol of PSA, 0.84 mmol of KOH in 20 mL of solvent, 130 °C and 30 bar Ar. [1]The data in EtOH was obtained from our previous work[18]; (B) Image for precipitated KS in IPA after PSA ring-opening and hydrolysis.

The KS synthesized in IPA exhibited the *trans*-2, *trans*-4 geometrical configuration, identical to that of commercially available KS (Fig. 7A-B). According to the literature, the *J* coupling constants of J_{H2H3}, J_{H3H4}, and J_{H4H5} of a *trans*-2, *trans*-4 KS were determined to be 15.3, 10.7, and 15.2 Hz, respectively.[58] In contrast, a *cis*-2, *trans*-4 configuration, observed in KS produced in EtOH, had the *J* coupling constants of 11.4, 11.6, and 14.3 Hz. Especially, the KS production in IPA was attractive with respect to the isolation of KS and the equivalent geometrical configuration of KS as the commercial one. Due to the distinctive properties of these isomers, further food safety evaluations are necessary with the *cis*-2, *trans*-4 as they could impact the safety profile and lead to unwanted effects.[34-37]

Only EtOH and IPA solvents were used in our study, making it challenging to explain the effect of solvents on the KS production from PSA in terms of solvent properties even though IPA is slightly less polar than EtOH and has higher steric hindrance. Nonetheless, this observation could serve as a clue for future research focused on selecting diverse solvents and examining the impact of the polarity, the ability to donate/accept protons, and the steric hindrance. Furthermore, the isomerization from the *cis*-2, *trans*-4 KS to the *trans*-2, *trans*-4 KS was not observed over time. Similarly, Carraher et al. investigated the effect of solvents on the isomerization of *cis-cis* Muconic acid, but *trans-trans* Muconic acid was not formed under conditions of 75°C and 14 days in various non-polar, polar protic and polar aprotic solvents.[59] Interestingly, the *trans- trans* Muconic acid was achieved at a yield of 54% only in Dimethyl sulfoxide-d6 under the same conditions. Accordingly, while the exact role of solvents remains unclear concerning the KS geometrical configuration, further investigation could offer valuable insights into the fundamental understanding of the KS production.

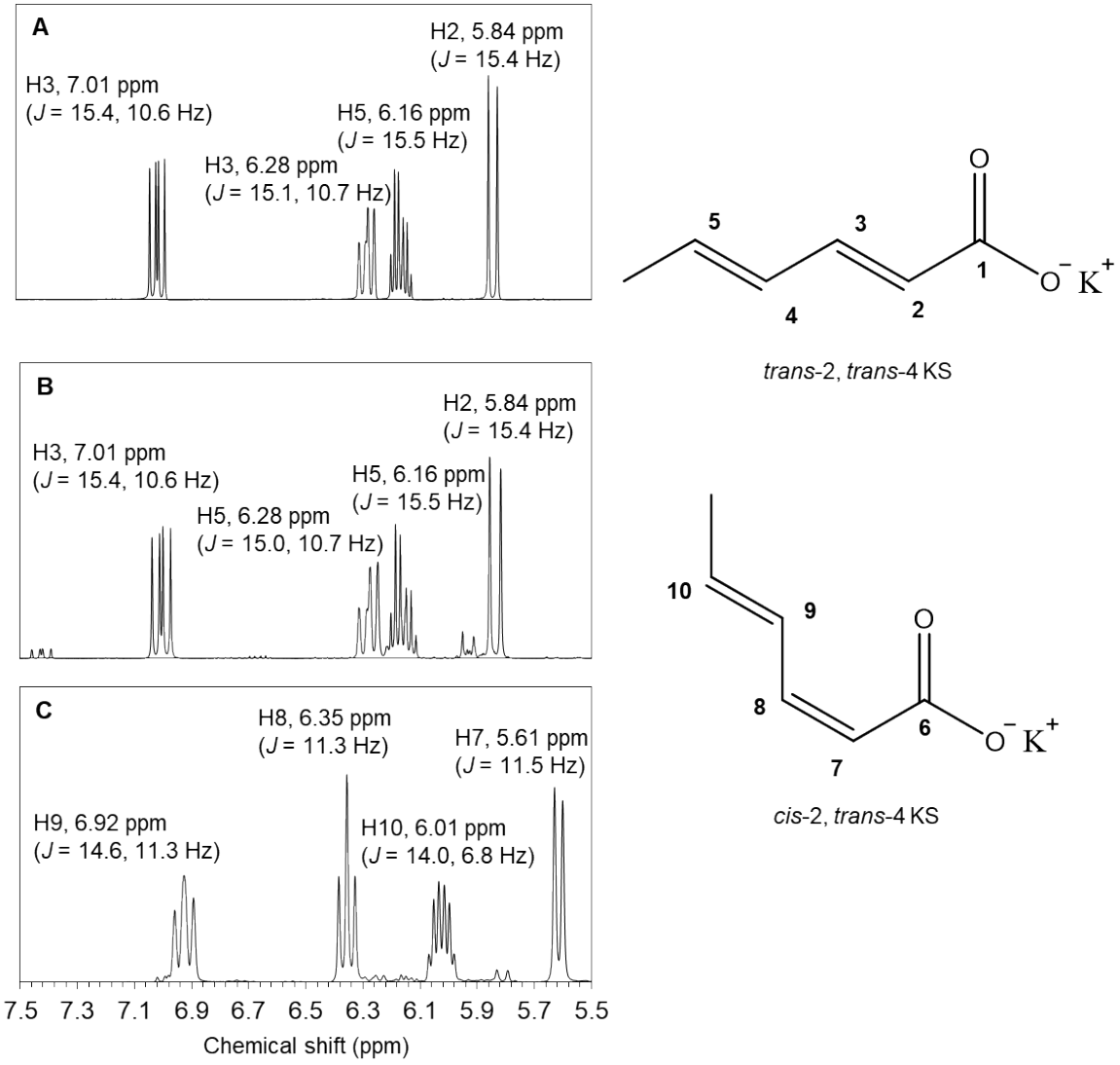

Fig. 7. ^{1}H NMR spectra of (A) commercial KS, (B) KS produced in IPA, and (C) KS produced in EtOH.

Overall process of KS production from TAL

Fig. 8 illustrates the overall process of producing KS from TAL, comparing both previous and current approaches. Reaction times and yields for hydrogenating TAL and producing PSA were calculated based on kinetic parameters, while the details for ring-opening and hydrolysis of PSA were determined using experimental data. Fig. 8A highlights the significant advancements made in producing KS from TAL using IPA, achieving an impressive yield of 87% in just 34.5 hours. This innovative approach with IPA not only maintains a comparable KS yield to that of the

previous method with THF but also reduces the process time by 5.5 hours, underscoring the enhanced efficiency and effectiveness of the proposed approach. This improvement was mainly attributed to the reduced duration required for PSA production, which decreased from 17.8 hours in THF to 6.1 hours in IPA, despite other reactions in IPA requiring longer durations. In the previous study[18], TAL hydrogenation with Ni/SiO_2 in THF was estimated to be 17 hours. According to the kinetic parameters obtained from this study, the complete TAL hydrogenation over Ni/Si-Al in THF was estimated to take 6.1 hours (Fig. S2 in ESI). This difference was due to the fact that the presence of the catalyst pretreatment.

In *Step 4* depicted in Fig. 8A, the precipitated KS was separated through a simple solid and liquid filtration, while the dissolved KS in solvent was obtained by evaporation. During this step, 0.46 mmol of KS was in IPA containing 6.7 mmol of H_2O. Given that the solubility of KS in H_2O is 58 g per 100 mL at 20°C, it implies that about 0.07 moles of KS could be dissolved in 1 mole of H_2O, and the solubility of KS in IPA was observed as negligible. It was assumed that 2% of product loss occurs in the purification step. Finally, impurities in the isolated KS were removed through an extraction method with IPA, and 6.6 mmol of KS having 95% of purity was produced from 7.0 mmol of TAL.

Furthermore, the process using THF and EtOH depicted in Fig. 8B, involved three solvent removal steps. Initially, THF was replaced with EtOH in *Step 3* to enhance the yield of KS in EtOH. Afterward, EtOH was evaporated to isolate KS that had dissolved within it (*Step 5*). Finally, THF was reintroduced for KS purification and subsequently recycled (*Step 6 and Step 7*). Therefore, the proposed approach employing IPA to produce KS from TAL not only reduced the total required reaction time, but also decreased the number of solvent recovery steps compared to the approach using THF and EtOH.

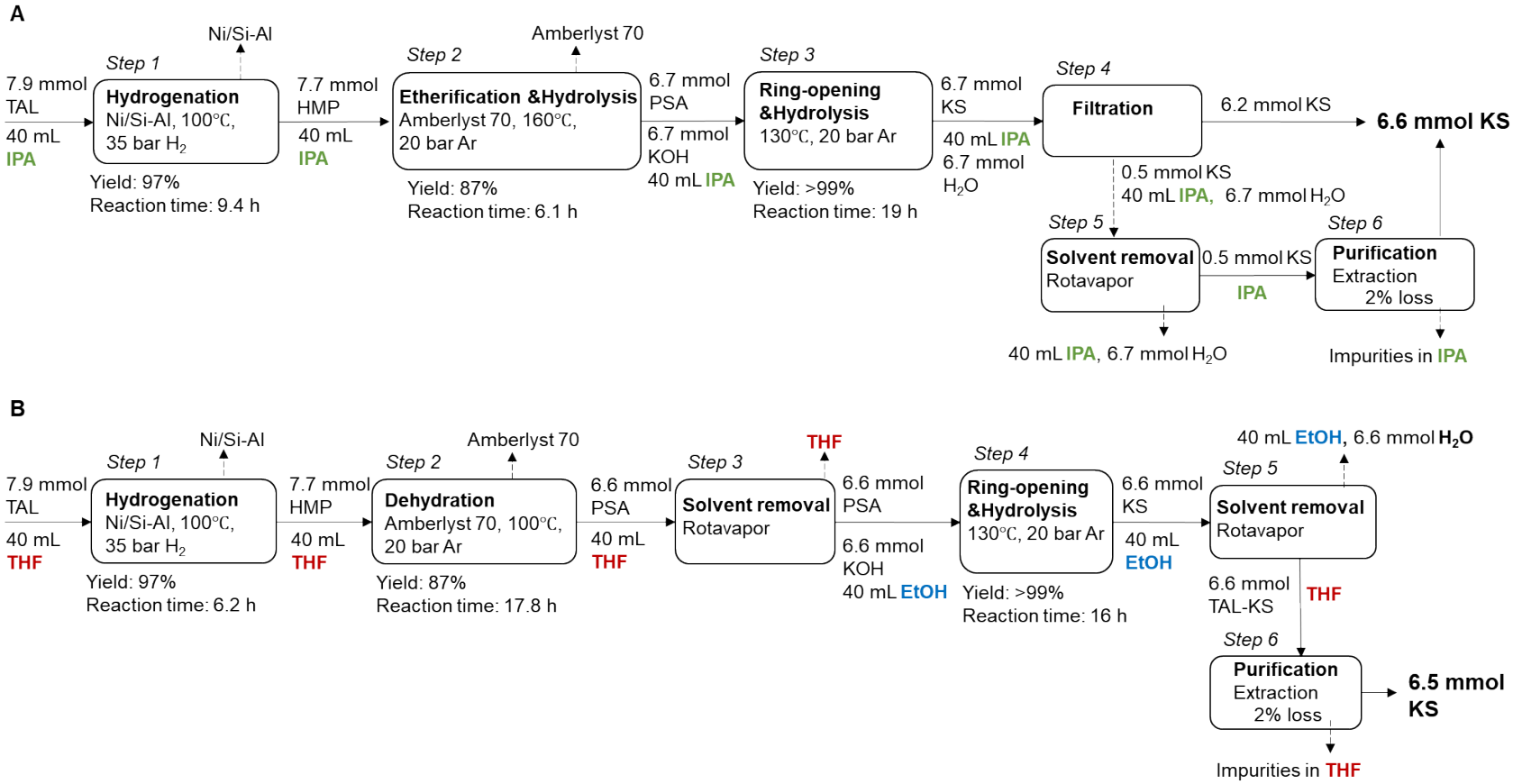

Fig. 8. Overall process of producing KS from TAL proposed in (A) this current study and (B) our previous study[18].

Techno-economic analysis and life cycle assessment of biorefineries producing KS via TAL from sugarcane

We designed end-to-end biorefineries that accepted sugarcane as a feedstock, microbially converted sugars (glucose and sucrose) present in sugarcane juice to TAL, and catalytically upgraded TAL to KS using either of the two developed reaction sequences (Fig. 8; simplified biorefinery block flow diagram shown in Fig. S6 in ESI; biorefinery design described in *Materials and Methods*).

For the current state-of-technology with the reaction sequence using IPA (*IPA* scenario; Fig. S6 in ESI), the biorefinery could produce KS with a baseline MPSP of \$8.27·kg^{-1} with a range of \$7.06−10.16·kg^{-1} [5th-95th percentiles from 6000 Monte Carlo simulations, hereafter shown in brackets] and a baseline CI of 13.7 [9.6−18.6] kg CO_2-eq·kg^{-1}. The MPSP and CI were both significantly reduced compared to those associated with biorefineries designed with the reaction sequence using THF and ethanol (\$9.68·kg^{-1} [\$8.47−11.45·kg^{-1}] and 16.2 [12.0−21.2] kg CO_2-eq·kg^{-1}, respectively, for the *THF & EtOH* scenario; Fig. S6 in ESI). This was mainly because: (i) the *IPA* scenario involved fewer solvent recovery steps than the *THF & EtOH* scenario (Fig. S6 in ESI), leading to decreased solvent losses and make-up solvent requirements (the make-up THF requirement was roughly 5-fold the make-up IPA requirement at the baseline, by mass); and (ii) the price and CI impact of purchasing IPA (\$1.07·kg^{-1} and 2.32 kg CO_2-eq·kg^{-1} IPA at the baseline, respectively) were significantly lower than for THF (\$4.45·kg^{-1} and 6.05 kg CO_2-eq·kg^{-1} THF, respectively; baseline values and uncertainty ranges for all parameters included in the uncertainty analysis are detailed in Tables S5 and S6 in the Supplementary Material). As a result, the cost and CI contributions from purchasing make-up IPA (2% of the biorefinery's annual material cost and 2% of total CI at the baseline for the *IPA* scenario) were significantly reduced relative to purchasing make-up THF (28% of the biorefinery's annual material cost and 18% of total CI for the *THF & EtOH* scenario). However, the MPSP for the *IPA* scenario was above the market range (\$5.03−6.50·kg^{-1}; Fig. 9A) in 99.5% of simulations, within the market range in 0.5% of simulations, and below the market range in none of the simulations for the current state-of-technology. In the absence of policy- or market-driven financial incentives for bioproducts, a

MPSP within or below the market range would be required to be competitive with the market for KS.

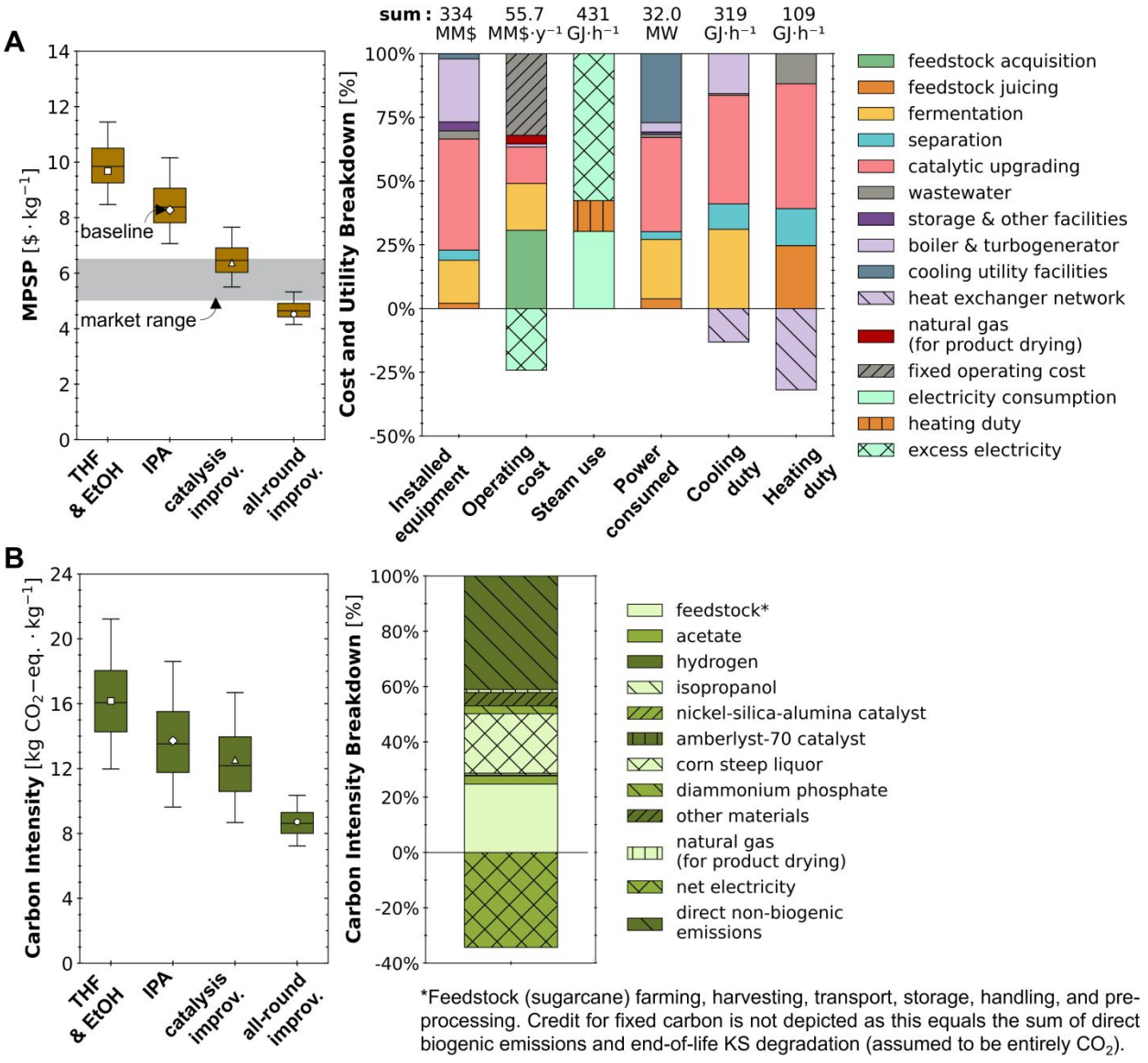

Fig. 9. Uncertainties (box-and-whisker plots) and breakdowns (stacked bar charts) for (A) minimum product selling price (MPSP) and (B) cradle-to-grave carbon intensity (CI) quantified as 100-year global warming potential (GWP_{100}) per kg of potassium sorbate (KS) produced by catalytic upgrading of TAL produced via microbial conversion of glucose, sucrose, and acetate by *Y. lipolytica*. *IPA* indicates results from TEA and LCA performed based on experimental data obtained in this study. Box and whisker plots show results for four scenarios: (i) current state-of-technology with THF and ethanol as solvents during catalytic upgrading (*THF & EtOH*; based on

experimental data from our previous study[18]); (ii) current state-of-technology with IPA as the solvent during catalytic upgrading (*IPA*; based on experimental data from this study); (iii) potential improvements over *IPA* to etherification and hydrolysis yield (to 96.9%), reaction times for hydrogenation (to 6.1 hours) and ring opening and hydrolysis (to 6.1 hours), and using continuous stirred-tank reactors for all three reactions (*catalysis improv.*); and (iv) potential improvements over *catalysis improv.* to fermentation TAL yield (to 73.0% of theoretical), TAL titer (to 65·gL^{-1}), and biorefinery annual operating time (to 240 days) with a potential decrease in TAL loss by ring-opening decarboxylation (to 4.8%) while increasing pH maintained by sodium hydroxide addition (to 11.0) during separation (*all-round improv.*). On box-and-whisker plots, whiskers, boxes, and the middle line represent 5^{th}/95^{th}, 25^{th}/75^{th}, and 50^{th} percentiles, respectively, from 6000 Monte Carlo simulations. Diamonds and stacked bar charts report results for baseline values for the *IPA* scenario. Square, triangle, and hexagon markers represent baseline values for the *THF & EtOH*, *catalysis improv.*, and *all-round improv.* Scenarios, respectively. The shaded gray region shows the market price range for KS ($5.03–6.50·$kg^{-1}$).[49, 60] For the biorefinery's operating cost (MM$·$y^{-1}$), contributions from fixed operating costs, sales revenue from excess electricity, purchase of natural gas for product drying, and material costs by process area are shown. *Installed equipment* cost indicates the total cost of purchasing and installing equipment. Values above stacked bars are totals (including offsets. For heating duty, cooling duty, and electricity consumption, values indicate totals during operation. Tabulated data breaking down capital and material costs, heating and cooling duties, electricity consumption, CI, and FEC are available online.[43]

Of the 50 parameters included in the uncertainty analysis for the current state-of-technology *IPA* scenario (Fig. 9), we found MPSP was highly sensitive to etherification and hydrolysis yield of PSA on HMP (Spearman's ρ of -0.30 and p-value<0.05). MPSP was also sensitive to hydrogenation yield of HMP on TAL (Spearman's ρ of -0.11 and p-value<0.05), and CI was sensitive to etherification and hydrolysis yield of PSA on HMP (Spearman's ρ of -0.18 and p-value<0.05; uncertainty distributions and Spearman's values for all parameters are listed in Table S5 and Fig. S8 in ESI, respectively), indicating the significance of the catalytic upgrading technological performance for system sustainability.

To enable the identification and pursuit of specific targets in catalytic upgrading of TAL to KS, we designed and simulated biorefineries across the theoretical catalytic upgrading performance space (i.e., 3600 potential combinations of yield and reaction time for each of the three reactors—hydrogenation, etherification and hydrolysis, and ring-opening and hydrolysis; Fig. 10) to quantify how future improvements to catalytic conversion would impact the sustainability of sugar-based TAL production.

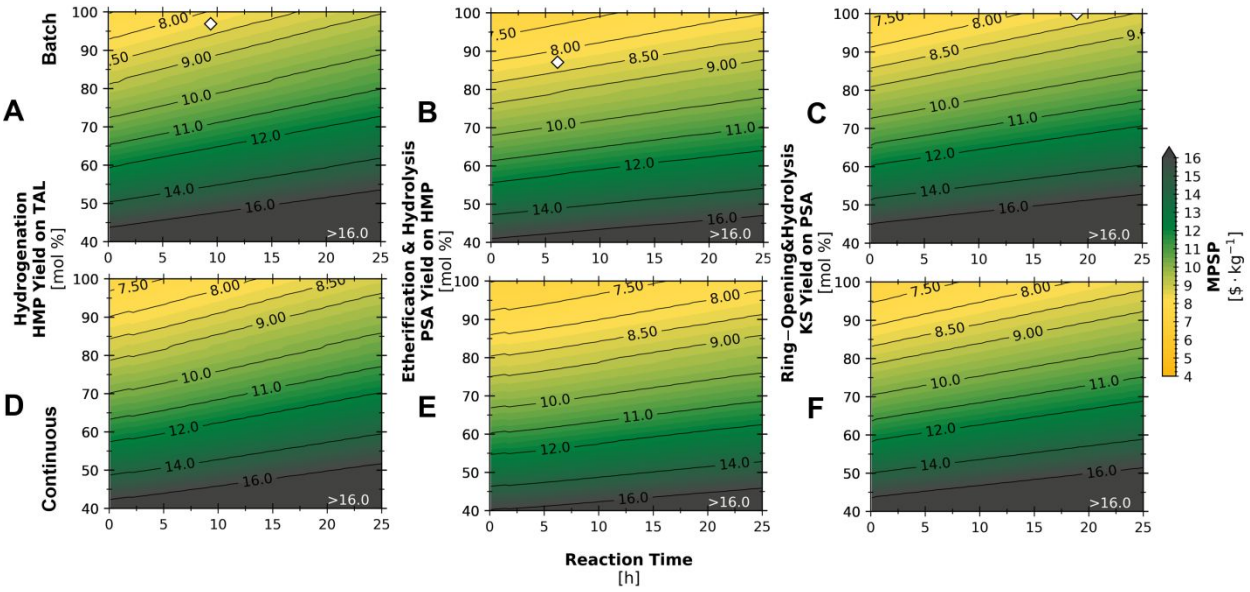

Fig. 10. Minimum product selling price (MPSP) of KS across theoretical product yields (*y*-axes) and reaction times (*x*-axes) for the (A,D) hydrogenation, (B,E) etherification and hydrolysis, and (C,F) ring-opening and hydrolysis reactors operating in batch (A,B,C) and continuous modes (D,E,F). For a given point on the figure, the *x-axis* value represents the reaction time (h), the *y-axis* value represents the yield (mol%) of HMP on TAL (A,D), PSA on HMP (B,E), or KS on PSA (C,F), and the color represents MPSP. The baseline product yield-reaction time combinations for each reactor are represented by diamonds (A,B,C).

Across the evaluated theoretical catalytic upgrading spaces for hydrogenation, etherification and hydrolysis, and ring-opening and hydrolysis, both MPSP (Fig. 10) and CI (Fig. S7 in ESI) benefited from increases in yields (of HMP, PSA, and KS, respectively) and decreases in reaction times. Greater yields resulted in higher KS production per mass of feed sugarcane, significantly reducing normalized costs; this was consistent with feed sugarcane acquisition being

the largest contributor (47% [39−55%]) to the biorefinery's annual material cost of 48.4 MM$·y^{-1} [37.6−62.2 MM$·y^{-1}] for the *IPA* scenario (Fig. 9A). Lower reaction times allowed smaller reaction vessel sizes and catalyst requirements, significantly reducing the total capital cost as well as catalyst recovery and make-up costs; this was consistent with the catalytic upgrading process being the largest contributor (44% [39−49%]) to the biorefinery's total equipment purchase and installation cost of 334 MM$ [267−432 MM$] for the *IPA* scenario (Fig. 9A). The minima for MPSP and CI in the evaluated spaces were \$7.48·kg^{-1} and 13.4 kg CO_2-eq·kg^{-1} (for hydrogenation), \$7.08·kg^{-1} and 12.3 kg CO_2-eq·kg^{-1} (for etherification and hydrolysis), and \$7.34·kg^{-1} and 13.3 kg CO_2-eq·kg^{-1} (for ring-opening and hydrolysis), respectively (Fig. 10A-C and Fig. S7A-C in ESI). The minima for MPSP were further reduced if reactors were operated in continuous rather than batch mode to \$7.29·kg^{-1} (for hydrogenation), \$6.98·kg^{-1} (for etherification and hydrolysis), and \$7.13·kg^{-1} (for ring-opening and hydrolysis; Fig. 10D-F), with the minima for CI remaining roughly the same as in batch mode operation (Fig. S7D-F in ESI). Operating reactors in continuous mode can enable significant reductions in the biorefinery's total equipment purchase and installation cost (e.g., from 334 MM$ at the baseline to 296 MM$) as fewer pressure vessels, agitators, recirculation pumps, heat exchangers, platforms, and ladders need to be purchased and installed relative to operating in batch mode with the same KS production. However, isolated improvements to any of these reactors would not be sufficient to compete with the market range (\$5.03−6.50·kg^{-1}), suggesting that combined improvements would be needed for financial viability and enhanced environmental sustainability.

As MPSP and CI were significantly sensitive to assumptions in technological parameters for catalytic upgrading (Fig. S8 in ESI), the following targeted improvements were explored to illustrate the potential benefits of additional catalysis research and development: (i) increase in etherification and hydrolysis yield (from 87 to 97%); (ii) decrease in hydrogenation reaction time (from 9.4 to 6.1 hours); and (iii) decrease in ring-opening and hydrolysis reaction time (from 19 to 6.1 hours). This scenario represented modest potential advancements in etherification and hydrolysis to achieve a yield on par with that achieved for hydrogenation (96.9%), and in hydrogenation as well as ring-opening and hydrolysis to achieve reaction times on par with that achieved for etherification and hydrolysis (6.1 hours). The resulting biorefinery's MPSP was

$6.38·kg^{-1}$ [$5.50–7.66·kg^{-1}$] and the CI was 12.5 [8.7–16.7] kg CO_2-eq·kg^{-1} (*catalysis improv.* scenario, Fig. 9). The MPSP was below the high end of the market range ($6.50·$kg^{-1}$) in 52.6% of simulations (compared to 0.5% for the current state-of-technology *IPA* scenario; Fig. 9).

Further, we observed MPSP and CI were significantly sensitive to assumptions in fermentation and separation technological parameters as well as the biorefinery's annual operating time (Fig. S8 in ESI). A previous study identified targeted improvements in the fermentation and separation processes combined with feed sweet sorghum integration that would significantly benefit the MPSP and CI of biorefineries producing TAL.[38] Based on the recommendations of that study, we explored the following potential improvements: (i) increases in fermentation TAL yield (to 73.0% of theoretical) and titer (to 65·gL^{-1}); (ii) increase in biorefinery annual operating time (to 240 days) by integrating sweet sorghum processing while maintaining the baseline production capacity of 15,940 metric ton KS·y^{-1}; (iii) decrease in TAL loss by ring-opening decarboxylation (to 4.8%) while increasing pH maintained by sodium hydroxide addition (to 11.0) during separation. If these improvements were achieved in addition to the above catalytic upgrading improvements, the resulting biorefinery's MPSP and CI would become $4.52·$kg^{-1}$ [$4.15–5.33·$kg^{-1}$] and 8.7 [7.2–10.4] kg CO_2-eq·kg^{-1} (*all-round improv.* scenario, Fig. 9), respectively. The MPSP of the produced KS was below the high end of the market range ($6.50·$kg^{-1}$) in 100.0% of simulations and below the low end of the market range ($5.03·$kg^{-1}$) in 83.4% of simulations, indicating a high potential for market-competitiveness. This highlights the potential for combined advancements in catalytic upgrading of TAL to KS, microbial conversion of sugars to TAL, TAL separation, and integrated processing of multiple feedstocks to significantly enhance the biorefinery's financial viability and environmental sustainability.

Conclusions

This study has successfully demonstrated a viable method for producing food-grade potassium sorbate (KS) from triacetic acid lactone (TAL) using isopropyl alcohol (IPA). In this study, KS production from TAL was achieved through a three-step process: 1) hydrogenation of TAL to HMP using a Ni/Si-Al catalyst, 2) etherification and hydrolysis of HMP to PSA using Amberlyst 70, and 3) ring-opening and hydrolysis of PSA with KOH as a co-reactant to produce KS. The product

selectivity and rate of formation were higher in IPA compared to EtOH. A reaction kinetics study was developed to find the optimal PSA yield from HMP in IPA. The KS yield from TAL in IPA reached 84% with this three-step process. The KS produced in this study exhibited a *trans*-2, *trans*-4 geometrical configuration identical to that of commercially available KS. This ensures that the KS produced is suitable for widespread use in food and pharmaceutical applications, maintaining its efficacy as a preservative. Although the effect of the solvent on the KS geometrical configuration is unknown, further research could provide important insights into the fundamental aspects of the KS production. In this study, we achieved comparable yields to previous research by utilizing green solvents. Remarkably, we also reduced the overall reaction time for producing PSA from HMP to just 6.2 hours using IPA, compared to the 17.8 hours required in the previous approach with THF. This reduction in reaction time enhances the process's economic efficiency.

Further, for the current state-of-technology, we found biorefineries leveraging the developed catalytic upgrading process with IPA as the solvent could produce KS from sugarcane with a MPSP of $\$8.27 \cdot kg^{-1}$ [$\$7.06–10.16 \cdot kg^{-1}$] and a CI of 13.7 [9.6–18.6] kg CO_2-eq$\cdot kg^{-1}$, with improved financial viability and environmental sustainability relative to biorefineries that used the previously developed process with THF and ethanol (MPSP of $\$9.68 \cdot kg^{-1}$ [$\$8.47–11.45 \cdot kg^{-1}$] and CI of 16.2 [12.0–21.2] kg CO_2-eq$\cdot kg^{-1}$). With potential targeted improvements in the catalytic upgrading process (an increase of 9.8% in etherification and hydrolysis yield of PSA; decreased reaction times for hydrogenation by 3.3 hours and for ring-opening and hydrolysis by 12.9 hours; operating all three reactors in continuous mode), the resulting MPSP of $6.38 \cdot kg^{-1}$ [$\$5.50–7.66 \cdot kg^{-1}$] was below the high end of the market price range ($\$6.50 \cdot kg^{-1}$) in 52.6% of Monte Carlo simulations. Finally, with combined potential improvements in the catalytic upgrading process (as above), the fermentation process (increased TAL yield to 73% of theoretical and TAL titer to 65.0 $g \cdot kg^{-1}$), the separation process (decreased TAL loss by ring-opening decarboxylation to 4.8% while maintaining a pH of 11.0 by sodium hydroxide addition), and integrated sweet sorghum processing (increasing the biorefinery's annual operating time to 240 days), the resulting biorefinery's CI was 8.7 [7.2–10.4] kg CO_2-eq$\cdot kg^{-1}$ and the MPSP was $\$4.52 \cdot kg^{-1}$ [$\$4.15–5.33 \cdot kg^{-1}$], which was below the high end of the market range ($\$6.50 \cdot kg^{-1}$) in all simulations and below the

low end of the market range ($5.03·kg^{-1}) in 83.4% of simulations, indicating a high potential for market-competitiveness with combined potential improvements along the KS value chain. While the developed KS production process could be financially viable for current state-of-technology assumptions under uncertainty, further experimental validation at larger scales will be needed to assess the potential to commercialize this process. Future studies will focus on developing regimes for continuous catalytic conversion of TAL to KS with further increased etherification and hydrolysis yield of PSA and decreased reaction times.

Author contributions

M.S.K., L.S-M., X.S., and K.C. contributed to data curation, formal analysis, investigation, methodology, validation, visualization, and writing; G.W.H contributed to conceptualization, project administration, funding acquisition, supervision, and writing; S.S.B. and J.S.G. performed the techno-economic analysis and life cycle assessment. All authors participated in discussing the data and ideas and contributed their input to the manuscript.

Data availability

The data supporting this article have been included as part of the ESI. All results for techno-economic analysis and life cycle assessment (including plots and raw data) and the software scripts used to generate the same are available at *BioSTEAMDevelopmentGroup: Triacetic acid lactone biorefineries, 2024* (https://github.com/BioSTEAMDevelopmentGroup/Bioindustrial-Park/tree/master/biorefineries/TAL).

Conflicts of interest

There are no conflicts to declare.

Acknowledgements

This work was funded by the DOE Center for Advanced Bioenergy and Bioproducts Innovation (U.S. Department of Energy, Office of Science, Office of Biological and Environmental Research under Award Number DE-SC0018420). Any opinions, findings, and conclusions or

recommendations expressed in this publication are those of the author(s) and do not necessarily reflect the views of the U.S. Department of Energy.

References

1 R. K. Srivastava, N. P. Shetti, K. R. Reddy, E. E. Kwon, M. N. Nadagouda and T. M. Aminabhavi, *Environ. Pollut.*, 2021, **276**, 116731.

2 R. S. Varma, *ACS Sustain. Chem. Eng.*, 2019, **7**, 6458-6470.

3 H. Chang, A. H. Motagamwala, G. W. Huber and J. A. Dumesic, *Green Chem.*, 2019, **21**, 5532-5540.

4 W. Leitner, J. Klankermayer, S. Pischinger, H. Pitsch and K. Kohse-Höinghaus, *Angew. Chem. Int. Ed.*, 2017, **56**, 5412-5452.

5 M. Cao, V. G. Tran, J. Qin, A. Olson, S. Mishra, J. C. Schultz, C. Huang, D. Xie and H. Zhao, *Biotechnol. Bioeng.*, 2022, **119**, 2529-2540.

6 J. W. Lee, S. Yook, H. Koh, C. V. Rao and Y.-S. Jin, *Curr. Opin. Biotechnol.*, 2021, **67**, 15-25.

7 P. B. Otoupal, G. M. Geiselman, A. M. Oka, C. A. Barcelos, H. Choudhary, D. Dinh, W. Zhong, H. Hwang, J. D. Keasling and A. Mukhopadhyay, *Microb. Cell Fact.*, 2022, **21**, 1-17.

8 R. Singh, S. S. Bhagwat, M. B. Viswanathan, Y. R. Cortés-Peña, K. K. Eilts, G. McDonough, M. Cao, J. S. Guest, H. Zhao and V. Singh, *Biofuels, Bioprod. Bioref.*, 2023, **17**, 109-120.

9 Y. Zhou, E. N. Mirts, S. Yook, M. Waugh, R. Martini, Y. S. Jin and Y. Lu, *Angew. Chem. Int. Ed.*, 2023, **62**, e202212440.

10 M. Chia, T. J. Schwartz, B. H. Shanks and J. A. Dumesic, *Green Chem.*, 2012, **14**, 1850-1853.

11 M. Chia, M. A. Haider, G. Pollock III, G. A. Kraus, M. Neurock and J. A. Dumesic, *J. Am. Chem. Soc*, 2013, **135**, 5699-5708.

12 G. Shrivastav, T. S. Khan, M. Agarwal and M. A. Haider, *React. Chem. Eng.*, 2020, **5**, 651-662.

13 J. H. F. de Jesus, I. M. Szilágyi, G. Regdon Jr and E. T. G. Cavalheiro, *Food Chem.*, 2021, **337**, 127770.

14 S. Salwan, I. Passi and B. Kumar, *Curr. Anal. Chem.*, 2022, **18**, 977-988.

15 F. Zappaterra, D. Summa, B. Semeraro, R. Buzzi, C. Trapella, M. Ladero, S. Costa and E. Tamburini, *Fermentation*, 2020, **6**, 96.

16 M. C. Robach and F. J. Ivey, *Journal of Food Protection*, 1978, **41**, 284-288.

17 E. Lück, *Food Additives & Contaminants*, 1990, **7**, 711-715.

18 M. S. Kim, D. Choi, J. Ha, K. Choi, J.-H. Yu, J. A. Dumesic and G. W. Huber, *ACS Catal.*, 2023, **13**, 14031-14041.

19 *US Food and Drug Administration, 21-CFR-173, Code of Federal Regulations Titile 21, Part 173-Secondary direct food additives permitted in food for human consumption, Available online: https://www.accessdata.fda.gov/scripts/cdrh/cfdocs/cfcfr/CFRSearch.cfm?CFRPart=173&showFR=1&subpartNode=21:3.0.1.1.4.3 (accessed 30 May 2024).*

20 B. Xu, *Adv. Mater. Res.*, 2013, **781**, 1328-1331.

21 J. J. Pang, Z. Q. Yao, K. Zhang, Q. W. Li, Z. X. Fu, R. Zheng, W. Li, J. Xu and X. H. Bu, *Angew. Chem.*, 2023, **135**, e202217456.

22 C.-Y. Gao, D. Wang, J.-P. Li, Y. Wang and W. Yang, *CrystEngComm*, 2016, **18**, 2857-2863.

23 H.-Y. Zheng, X. Lian, S.-j. Qin and B. Yan, *Dalton Trans.*, 2018, **47**, 6210-6217.

24 R. Hussain, M. Q. Khan and A. A. Khan, *J. Ind. Eng. Chem.*, 2019, **70**, 186-195.

25 G. A. Dannan, *Hamilton & Hardy's Industrial Toxicology*, 2015, 719-726.

26 C. Capello, U. Fischer and K. Hungerbühler, *Green Chem.*, 2007, **9**, 927-934.

27 P. G. Jessop, *Green Chem.*, 2011, **13**, 1391-1398.

28 S. M. Jain, T. Edvinsson and J. R. Durrant, *Commun. Chem.*, 2019, **2**, 91.

29 E. Yara-Varon, A.-S. Fabiano-Tixier, M. Balcells, R. Canela-Garayoa, A. Bily and F. Chemat, *RSC Adv.*, 2016, **6**, 27750-27759.

30 W. Xie, T. Li, C. Chen, H. Wu, S. Liang, H. Chang, B. Liu, E. Drioli, Q. Wang and J. C. Crittenden, *Ind. Eng. Chem. Res.*, 2019, **58**, 6413-6423.

31 *US Food and Drug Administration, 21-CFR-184.1293, Code of Federal Regulations Title 21, Ethyl alcohol, Available online: https://www.ecfr.gov/current/title-21/chapter-I/subchapter-B/part-184/subpart-B/section-184.1293 (accessed 30 May 2024).*

32 *US Food and Drug Administration, 21-CFR-173.240, Code of Federal Regulations Title 21, Isopropyl alcohol. Available online: https://www.ecfr.gov/current/title-21/chapter-I/subchapter-B/part-173/subpart-C/section-173.240 (accessed 30 May 2024).*

33 *US Food and Drug Administration, 21-CFR-178.1010, Code of Federal Regulations Title 21, Part 178-Indirect food additves: adjuvants, production adis, and sanitizers, Available online: https://www.accessdata.fda.gov/scripts/cdrh/cfdocs/cfcfr/CFRSearch.cfm?fr=178.1010 (accessed 30 May 2024).*

34 C. J. Zhang, G. Feng, S. Xu, Z. Zhu, X. Lu, J. Wu and B. Liu, *Angew. Chem.*, 2016, **128**, 6300-6304.

35 J. Liang, H. Shi, R. T. Kwok, M. Gao, Y. Yuan, W. Zhang, B. Z. Tang and B. Liu, *J. Mater. Chem. B*, 2014, **2**, 4363-4370.

36 J. Witkin, J. Kranzler, K. Kaniecki, P. Popik, J. Smith, K. Hashimoto and J. Sporn, *Pharmacol. Biochem. Behav.*, 2020, **194**, 172927.

37 N. Chhabra, M. L. Aseri and D. Padmanabhan, *Int. J. Appl. Basic Med. Res.*, 2013, **3**, 16.

38 S. S. Bhagwat, M. N. Dell'Anna, Y. Li, C. Mingfeng, E. C. Brace, S. S. Bhagwat, G. W. Huber, H. Zhao and J. S. Guest, *ChemRxiv. doi:10.26434/chemrxiv-2024-4sz8x-v2. This content is a preprint and has not been peer-reviewed.*, 2024.

39 *BioSTEAM Development Group, BioSTEAM: The Biorefinery Simulation and Techno-Economic Analysis Modules., (2024). Available online: https://github.com/BioSTEAMDevelopmentGroup/biosteam (accessed June 14, 2024).*

40 Y. Cortes-Pena, D. Kumar, V. Singh and J. S. Guest, *ACS Sustain. Chem. Eng.*, 2020, **8**, 3302-3310.

41 Y. Cortés-Peña, *J. Open Source Softw.*, 2020, **5**, 2814.

42 *BioSTEAM Development Group. Thermosteam: BioSTEAM's Premier Thermodynamic Engine., (n.d.). Available online: https://github.com/BioSTEAMDevelopmentGroup/thermosteam (accessed June 14, 2024).*

43 *BioSTEAMDevelopmentGroup, Triacetic acid lactone biorefineries, (2024). Available online: https://github.com/BioSTEAMDevelopmentGroup/Bioindustrial-Park/tree/master/biorefineries/TAL (accessed June 17, 2024).*

44 *Transparency Market Research, Sorbic Acid Market: Global Industry Analysis, Size, Share, Growth, Trends, and Forecast, 2019–2030, 2020.*

45 *E. de Sousa, I. de C. Macedo, Ethanol and bioelectricity: sugarcane in the future of the energy matrix, São Paulo: UNICA (2010).*

46 Y. Cortés-Peña, C. Kurambhatti, K. Eilts, V. Singh and J. S. Guest, *ACS Sustain. Chem. Eng.*, 2022, **10**, 13980-13990.

47 H. Huang, S. P. Long, T. E. Clemente and V. Singh, *Ind. Biotechnol.*, 2016, **12**, 357-365.

48 H. Huang, S. Long and V. Singh, *Biofuels, Bioprod. Bioref.*, 2016, **10**, 299-315.

49 *Alibaba.com, Lifecare Supply Potassium Sorbate High Quality Potassium Sorbate Granular - Shaanxi Lifecare Biotechnology Co., Ltd, (n.d.). Available online: https://www.alibaba.com/product-detail/Lifecare-Supply-Potassium-Sorbate-High-Quality_1600897125355.html (accessed June 17, 2024).*

50 *U.S. EPA, Lifecycle Analysis of Greenhouse Gas Emissions under the Renewable Fuel Standard, (n.d.). Available online: https://www.epa.gov/renewable-fuel-standard-program/lifecycle-analysis-greenhouse-gas-emissions-under-renewable-fuel (accessed June 17, 2024).*

51 *I. WG, The physical science basis, Contribution of Working Group I to the Fifth Assessment Report of the Intergovernmental Panel on Climate Change 1535 (2013).*

52 *Argonne National Laboratory. GREET 2020 Model. October 10, 2020., (n.d.).*

53 G. Wernet, C. Bauer, B. Steubing, J. Reinhard, E. Moreno-Ruiz and B. Weidema, *Int. J. Life Cycle Assess.*, 2016, **21**, 1218-1230.

54 M. C. Allen, A. J. Hoffman, T.-w. Liu, M. S. Webber, D. Hibbitts and T. J. Schwartz, *ACS Catal.*, 2020, **10**, 6771-6785.

55 J. Rorrer, S. Pindi, F. D. Toste and A. T. Bell, *ChemSusChem*, 2018, **11**, 3104-3111.

56 J. M. Khurana, S. Chauhan and G. Bansal, *Monatsh. Chem.*, 2004, **135**, 83-87.

57 G. Fridkin, I. Columbus, L. Yehezkel and Y. Zafrani, *J. Org. Chem.*, 2018, **83**, 10541-10545.

58 I. K. Cigić, J. Plavec, S. S. Možina and L. Zupančič-Kralj, *J. Chromatogr. A*, 2001, **905**, 359-366.

59 J. M. Carraher, T. Pfennig, R. G. Rao, B. H. Shanks and J.-P. Tessonnier, *Green Chem.*, 2017, **19**, 3042-3050.

60 *Sorbic Acid Market. Global Industry Analysis, Size, Share, Growth, Trends, and Forecast, 2019–2030 (2020). Available online: https://www.transparencymarketresearch.com/sorbic-acid-market.html (accessed June 17, 2024).*

Data availability

The data supporting this article have been included as part of the ESI. All results for techno-economic analysis and life cycle assessment (including plots and raw data) and the software scripts used to generate the same are available at *BioSTEAMDevelopmentGroup: Triacetic acid lactone biorefineries, 2024* (https://github.com/BioSTEAMDevelopmentGroup/Bioindustrial-Park/tree/master/biorefineries/TAL).